

Structural phase transition in the two-dimensional triangular lattice antiferromagnet $\text{RbFe}(\text{MoO}_4)_2$

S. A. Klimin, M. N. Popova, and B. N. Mavrin

Institute of Spectroscopy, Russian Academy of Sciences, 142190 Troitsk, Moscow region, Russia

P. H. M. van Loosdrecht

Material Science Center, University of Groningen, Nijenborgh 4, 9747 AG Groningen, The Netherlands

L. E. Svistov, A. I. Smirnov, and L. A. Prozorova

P. L. Kapitza Institute for Physical Problems, Russian Academy of Sciences, 117334 Moscow, Russia

H.-A. Krug von Nidda, Z. Seidov, and A. Loidl

Experimentalphysik V, Electronic Correlations and Magnetism, Institute of Physics, University of Augsburg, D-86135 Augsburg, Germany

A. Ya. Shapiro and L. N. Demianets

Institute of Crystallography, Russian Academy of Sciences, 117924 Moscow, Russia

(Received 31 December 2002; revised manuscript received 11 June 2003; published 7 November 2003)

We report temperature-dependent x-ray powder diffraction patterns and single-crystal electron spin resonance (ESR) and Raman spectra of the two-dimensional triangular-lattice antiferromagnet $\text{RbFe}(\text{MoO}_4)_2$. A structural phase transition is found to occur in this compound at $T_c \approx 190$ K. By analyzing our data and the literature data on similar compounds, we conclude that the 190 K transition comprises rotations of MoO_4 tetrahedra and is, most likely, a transformation from a highly symmetric $P\bar{3}m1$ room-temperature structure into a very similar but less symmetric $P\bar{3}c1$ low-temperature one. The shift of the ESR frequency and the ESR linewidth were found to be determined by the crystal field influence and are described well considering the single-ion anisotropy with the constant $D/k_B = 0.25$ K. The change of the crystal field at the iron site below the phase-transition point T_c is estimated.

DOI: 10.1103/PhysRevB.68.174408

PACS number(s): 61.10.-i, 61.18.-j, 78.30.-j

I. INTRODUCTION

Two-dimensional (2D) triangular-lattice antiferromagnets are of interest in connection with the problem of magnetic ordering in frustrated spin systems. $\text{RbFe}(\text{MoO}_4)_2$ is a rare example of a nearly 2D “triangular” antiferromagnet suitable for magnetic measurements and available in single-crystal form.

$\text{RbFe}(\text{MoO}_4)_2$ belongs to the family of layered trigonal molybdates and tungstates with the structure of $\text{KAl}(\text{MoO}_4)_2$ type.¹ Magnetic Fe^{3+} ions situated inside FeO_6 octahedra form triangular-lattice layers that run perpendicular to the c axis and are separated by the successive MoO_4 , Rb , and MoO_4 layers (see Fig. 1). Isolated MoO_4 tetrahedra share common vertices with isolated FeO_6 octahedra, so that the shortest exchange paths between neighboring Fe^{3+} ions (situated at a distance equal to the unit-cell parameter $a = 5.69$ Å) go through two oxygen ions. The nearest Fe^{3+} ions in different layers are placed at a distance of the unit-cell parameter $c = 7.48$ Å and are interconnected through three or even four oxygens. The space group of $\text{RbFe}(\text{MoO}_4)_2$ at room temperature is $P\bar{3}m1$ (D_{3d}^3 , $Z = 1$).¹⁻³

Magnetic properties of the ordered state found below the Néel temperature $T_N = 3.8$ K were studied in Refs. 4, 5. Spins of the Fe^{3+} ions are arranged at 120° apart forming three magnetic sublattices within a layer of magnetic ions.

The behavior of the magnetization and ESR spectra correspond roughly to that of a planar antiferromagnet with the “triangular” magnetic structure. Nevertheless, a weak interplane interaction gives rise to additional phase transitions and spin-wave modes. Moreover, the magnetic structure appears to be incommensurate in the c direction (perpendicular to magnetic planes).⁶ The nature of the incommensurate modulation of the magnetic structure is still unknown.

Several members of the aforementioned family of trigonal molybdates and tungstates undergo structural phase transitions with temperature.⁷ As far as we know, the crystal structure of $\text{RbFe}(\text{MoO}_4)_2$ was investigated only at room temperature.

The knowledge of the distinct crystal structure is of importance for the explanation of the incommensurate magnetic structure, because the appropriate phase transitions are symmetry sensitive (see, e.g., Ref. 8). In this work, we study the temperature-dependent peculiarities of the structure of $\text{RbFe}(\text{MoO}_4)_2$ using x-ray diffraction, electron spin resonance (ESR), and Raman scattering.

II. EXPERIMENT

Single crystals of $\text{RbFe}(\text{MoO}_4)_2$ were grown by a flux method described in Ref. 3. Greenish, transparent thin crystals with typical dimensions of $2 \times 2 \times 0.2$ mm³ were obtained.

X-ray diffraction data were collected on powder samples

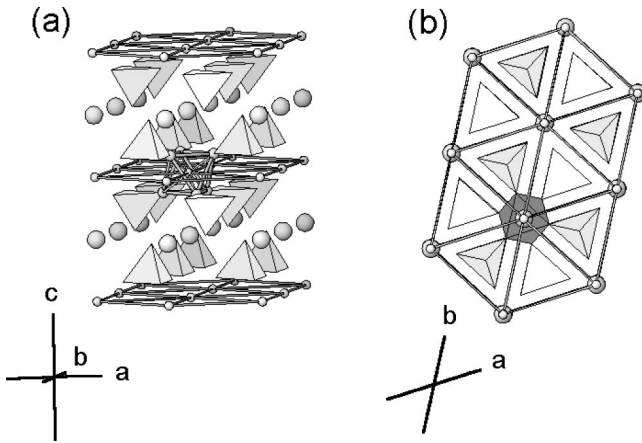


FIG. 1. Crystal structure of $\text{RbFe}(\text{MoO}_4)_2$. Fe and Rb atoms are represented by small and, correspondingly, big balls. Mo atoms reside within MoO_4 tetrahedra (light-gray). Only one FeO_6 octahedron is shown. (a) A general view. (b) $[001]$ view.

prepared from single crystals, at the temperatures 300, 250, 200, 180, 150, and 100 K. $\text{CuK}\alpha$ radiation was monochromatized by a curved germanium crystal. The indexing of the powder x-ray patterns was made using the program WINXPOW-1999. ESR measurements in the temperature range $4.2 \leq T \leq 300$ K were performed with a Bruker ELEXSYS E500CW spectrometer at X -band and Q -band frequencies (9.5 and 34 GHz, respectively). The spectrometer was equipped with an Oxford Instruments continuous He flow cryostat. The magnetic susceptibility at the temperatures between 1.8 and 300 K was measured with a SQUID magnetometer (Quantum Design).

Raman scattering was excited by the 514-nm line of an Ar-ion laser. Raman spectra at room temperature were measured in the Institute of Spectroscopy, employing a homemade triple spectrograph and a multichannel system consisting of an image-intensifier tube with a multichannel plate and a vidicon. The temperature-dependent Raman spectra were taken in the University of Groningen using a SPEX 14018 spectrometer and a Burle C13-34 photomultiplier. The typical laser power in these experiments was 20 mW. A single crystal of $\text{RbFe}(\text{MoO}_4)_2$ was attached to a copper sample holder by a silver paste and was placed into a closed-cycle He cryostat. The temperature of the holder near the sample location was measured with the aid of a silicon diode and could be varied between 33 and 300 K. Most of the samples strongly depolarize the light, so it was difficult to perform polarization measurements. Partially polarized Raman scattering in $z(xx)y$ and $z(xz)y$ configurations has been measured from a selected sample at room temperature.

III. RESULTS

A. X-ray powder diffraction

Powder x-ray diffraction patterns taken at 300 and 100 K are shown in Fig. 2(a). These patterns are similar one to another, the last one demonstrates some shift to larger angle values. At 180 K and, to a less extent, at 150 K several reflections became asymmetric. The temperature dependence

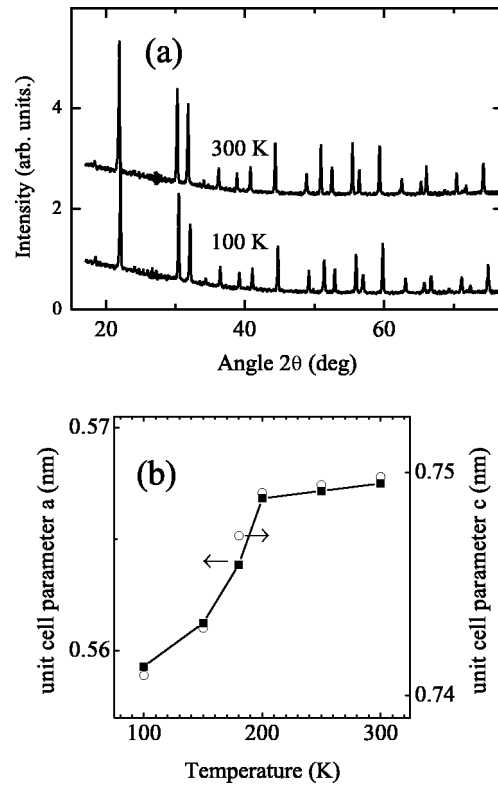


FIG. 2. Powder x-ray diffraction patterns of $\text{RbFe}(\text{MoO}_4)_2$ at 300 and 100 K (a) and crystallographic cell parameters a (filled squares) and c (open circles) as a function of temperature (b).

of the unit-cell parameters a and c display a peculiarity near 200 K pointing to a phase transition [see Fig. 2(b)]. Unfortunately, the accuracy of our x-ray experiment at low temperatures did not allow to make a choice between the close space groups $P\bar{3}m1$ and $P\bar{3}c1$.

B. Electron spin resonance

At temperatures higher than the Néel temperature, the ESR spectrum of the $\text{RbFe}(\text{MoO}_4)_2$ crystal consists of a single exchange-narrowed Lorentzian line with a resonance field corresponding to a g factor near $g \approx 2$. Figure 3 illustrates the results obtained at the microwave frequency 9.48 GHz (X band). The upper frame shows the temperature dependence of the resonance linewidth ΔH [here ΔH is the half-width at half maximum (HWHM)]. Since the linewidth is of the same order of magnitude as the resonance field (shown in the lower frame), the spectra were evaluated taking into account both circular components of the resonance, as described, e.g., in Ref. 9. The linewidth exhibits a pronounced anisotropy with respect to the crystallographic c axis. For the external magnetic field H applied parallel to the c axis ($\theta = 0^\circ$), the width is two times larger (1.5 kOe at room temperature) than for the magnetic field applied within the basal plane ($\theta = 90^\circ$), where it remains unchanged on rotation about the c axis. With decreasing temperature, the linewidth gradually increases and finally, near T_N , demonstrates a rapid growth typical for a critical behavior. Focusing on the phase transition near 200 K, where the lattice

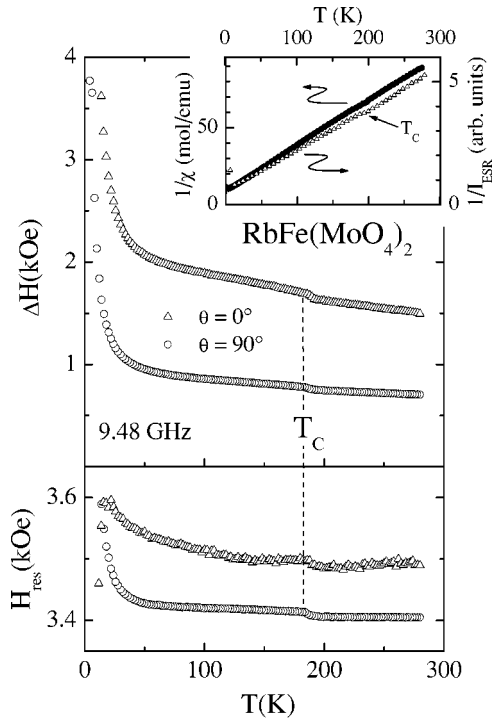


FIG. 3. Temperature dependence of the 9.48 GHz ESR linewidth (upper frame) and the resonance field (lower frame) in $\text{RbFe}(\text{MoO}_4)_2$ for the magnetic field applied parallel ($\theta=0^\circ$) and perpendicular ($\theta=90^\circ$) to the crystallographic c axis. Inset: temperature dependence of the inverse ESR intensity $1/I_{\text{ESR}}$ compared to the inverse static susceptibility $1/\chi$.

constant changes, we observe a distinct step of about 4% in the linewidth at $T_c=190$ K. At the same temperature, the resonance field H_{res} , which remained nearly unchanged above 50 K, exhibits a shift of approximately 1%. The inverse ESR intensity $1/I_{\text{ESR}}$ agrees well with the Curie-Weiss law found for the inverse susceptibility $1/\chi$ from SQUID measurements, as depicted in the inset of Fig. 3. Both show a slight kink near T_c , as well.

The critical line broadening on approaching T_N indicates an increasing importance of short-range order effects below 50 K. These effects give rise to fluctuating internal fields, which are independent of the external field, and which shift the resonance field. This shift is added to the paramagnetic shift due to the single ion anisotropy, and will be discussed below. To separate both contributions to the resonance shift, we performed additional ESR measurements at a higher microwave frequency of 34 GHz (Q band). Figure 4 shows the temperature dependences of the resonance field (lower frame) and of the linewidth (upper frame) for both main orientations of the magnetic field at 34 GHz. The linewidth data agree well with those obtained at 9.48 GHz (see inset). The anisotropy of the resonance field increases with decreasing temperature. The clear decrease of the resonance field observed at 34 GHz for the magnetic field applied in the basal plane was not detected at 9.48 GHz, but just the opposite behavior was observed resulting from the dominance of the short-range order in low external fields. However, at 34

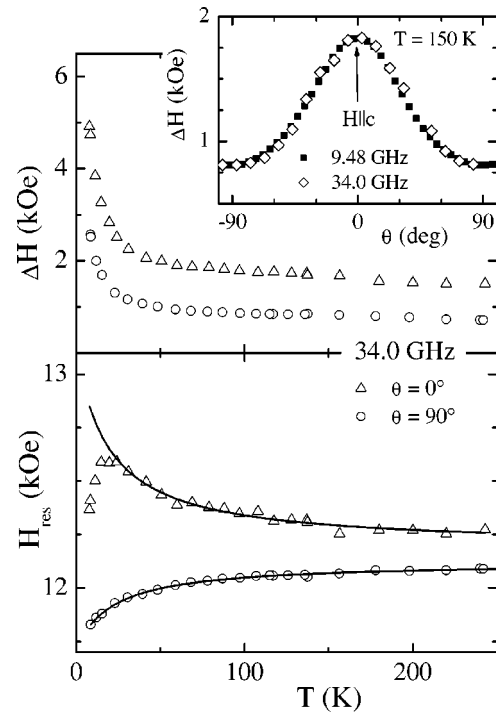


FIG. 4. Temperature dependence of the 34 GHz ESR linewidth (upper frame) and the resonance field (lower frame) in $\text{RbFe}(\text{MoO}_4)_2$ for the magnetic field applied parallel ($\theta=0^\circ$) and perpendicular ($\theta=90^\circ$) to the crystallographic c axis. The solid line is obtained from the fit described in the discussion. Inset: Angular dependence of the linewidth at 150 K for both X - and Q -band frequencies.

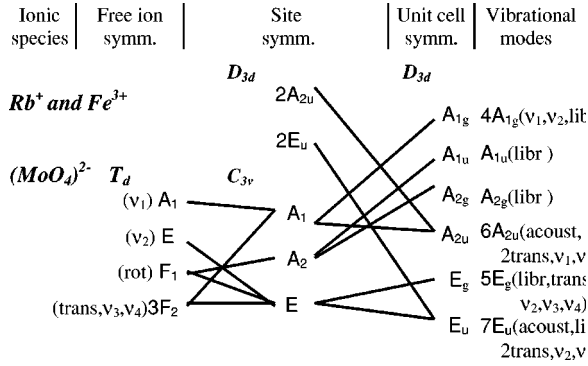
GHz the paramagnetic shift governs the resonance position due to the higher external field.

C. Group-theoretical analysis of vibrational modes

$\text{RbFe}(\text{MoO}_4)_2$ contains one formula unit ($N=12$ atoms) in a primitive cell of the trigonal space group $P\bar{3}m1$. Thus, there are $3N-3=33$ optical vibrations. To determine their symmetries, we perform a nuclear-site group analysis.¹⁰ Table I displays the crystallographic positions occupied by different atoms and the contributions from these atoms to the vibrational modes of the crystal. The atomic position is indicated according to the Wyckoff notation. The number of equivalent sites is given by a number before the letter nota-

TABLE I. Crystallographic positions occupied by different atoms and corresponding contributions to the vibrational modes of $\text{RbFe}(\text{MoO}_4)_2$, $P\bar{3}m1$ space group.

Atom position	Local symm.	Vibrational modes	
Rb	1b	D_{3d}	$A_{2u} + E_u$
Fe	1a	D_{3d}	$A_{2u} + E_u$
Mo	2d	C_{3v}	$A_{1g} + A_{2u} + E_g + E_u$
O1	2d	C_{3v}	$A_{1g} + A_{2u} + E_g + E_u$
O2	6i	C_s	$2A_{1g} + A_{1u} + A_{2g} + 2A_{2u} + 3E_g + 3E_u$

FIG. 5. Correlation scheme for vibrations of $\text{RbFe}(\text{MoO}_4)_2$.

tion. The local symmetry of an atomic position is indicated by the point-group symbol (in Schönflies notation). We note that there are two nonequivalent oxygen atoms O1 and O2. O1 atoms reside directly above (or below), Mo atoms in the MoO_4 tetrahedra, whereas O2 atoms are in the basal plane. Summarizing the contributions from all the atoms and subtracting the acoustic modes ($A_{2u} + E_u$), we obtain the following optical vibrational modes of $\text{RbFe}(\text{MoO}_4)_2$:

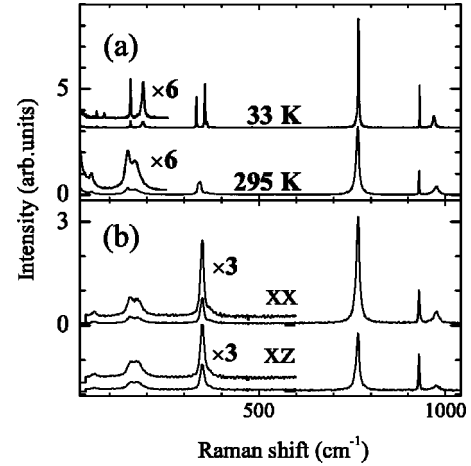
$$\Gamma^{\text{opt}}(P\bar{3}m1) = 4A_{1g}(xx,yy,zz) + A_{2g} + 5E_g(xz,yz,xy) + A_{1u} + 5A_{2u}(E||z) + 6E_u(E||x,E||y). \quad (1)$$

There are 9 Raman ($4A_{1g} + 5E_g$) and 11 infrared ($5A_{2u} + 6E_u$) modes. Note that the space group of $\text{RbFe}(\text{MoO}_4)_2$ contains the inversion operation and therefore Raman and infrared modes are well separated. Even (*g*) vibrations are Raman active, whereas the odd (*u*) ones are infrared active. A_{2g} and A_{1u} modes are silent.

Numerous studies of different molybdates have shown that a part of the crystal vibrations may be identified with the internal motions of the “free” $(\text{MoO}_4)^{2-}$ tetrahedral ion (which has T_d symmetry), $\nu_1(A_1)$, $\nu_2(E)$, $\nu_3(F_2)$, and $\nu_4(F_2)$.^{11,12} As usual, *A*, *E*, and *F* letters refer to nondegenerate, doubly and triply degenerate vibrations, respectively. To show the origin of the crystal lattice vibrations, we construct a correlation scheme for $\text{RbFe}(\text{MoO}_4)_2$ (see Fig. 5). The C_{3v} site symmetry of the MoO_4 ion splits the triply degenerate ν_3 and ν_4 vibrations ($F_2 \rightarrow A_1 + E$). The presence of two molybdate ions in the primitive cell, interacting with each other, results in the additional Davydov (or factor group) splitting, namely, $\nu_3, \nu_4(F_2) \rightarrow (A_{1g} + A_{2u}) + (E_g + E_u)$. Note, that the motions of Rb and Fe atoms do not manifest themselves in the Raman spectra.

D. Raman spectra

Figure 6(a) displays unpolarized Raman spectra of $\text{RbFe}(\text{MoO}_4)_2$ at room temperature and at 33 K. Below in this section, the temperatures of the sample holder are indicated and the heating of the sample by laser light is not taken into account. The room-temperature spectrum consists of nine lines, which is consistent with the $P\bar{3}m1$ space group. Table II gives the assignments of Raman modes deduced from the partially polarized spectra [see Fig. 6(b)] and from

FIG. 6. Unpolarized Raman spectra of $\text{RbFe}(\text{MoO}_4)_2$ at room temperature and 33 K (a) and room temperature partially polarized spectra (b).

a comparison with literature data on similar compounds¹¹ and on aqueous solution of $(\text{MoO}_4)^{2-}$, Ref. 12.

All the Raman lines shift and narrow with decreasing temperature (see Fig. 7). The temperature dependences of the line positions (Fig. 8) and linewidths (Fig. 9) show a specific feature at $T_c \approx 180$ K that evidences a phase transition. In particular, the distance between the two strong lines ($A_{1g} + E_g$) originating from the $\nu_4(F_2)$ vibration of the $(\text{MoO}_4)^{2-}$ tetrahedron, grows below the transition temperature, reflecting an additional distortion of the mentioned tetrahedron. The local C_{3v} symmetry of $(\text{MoO}_4)^{2-}$ either does not lower or lowers to C_3 (no splitting of the doubly degenerate components of the ν_4 or ν_3 vibrations is observed).

In the lowest-frequency region of the Raman spectra a new line near 80 cm^{-1} appears in the low-temperature spectrum [Figs. 6(a) and 7(a)]. This line strongly broadens and shifts to lower frequencies when approaching T_c from below [see Figs. 7(a), 8(a), and 9(a)].

IV. DISCUSSION

The Raman, ESR, and x-ray diffraction data point to a structural phase transition in $\text{RbFe}(\text{MoO}_4)_2$ at $T_c \approx 190$ K.

TABLE II. Raman modes of $\text{RbFe}(\text{MoO}_4)_2$ at room temperature.

Frequency (cm^{-1})	Symmetry	Assignment
977	A_{1g}	$\nu_1(A_1)$ vibration of MoO_4^{2-} (T_d)
930	E_g	$\nu_3(F_2)$ vibration of MoO_4^{2-} (T_d)
765	A_{1g}	
360	E_g	$\nu_2(E)$ vibration of MoO_4^{2-} (T_d)
343	E_g	$\nu_4(E)$ vibration of MoO_4^{2-} (T_d)
338	A_{1g}	
168	E_g	translational motions of MoO_4^{2-}
150	A_{1g}	
51	E_g	librational motion of MoO_4^{2-}

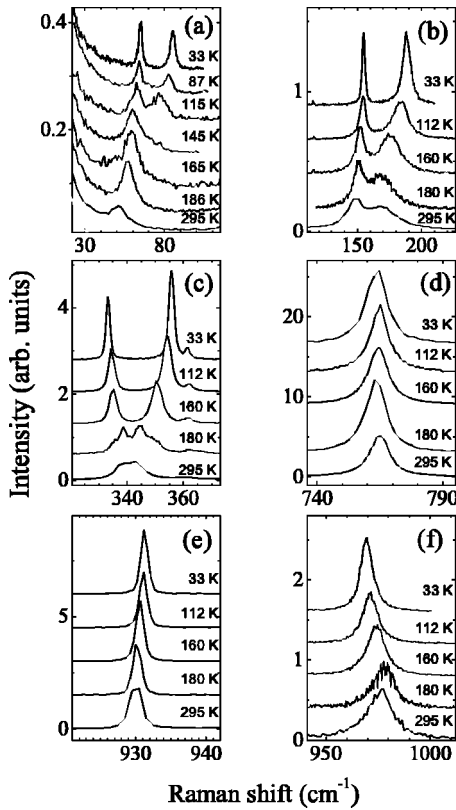


FIG. 7. Raman lines of $\text{RbFe}(\text{MoO}_4)_2$ at different temperatures.

(In view of the temperature $T_c \approx 180$ K that follows from Raman measurements a heating of the sample by laser light should be about 10 K which seems to be reasonable.) The Raman spectrum does not change qualitatively below T_c , except for the appearance of one new low-frequency mode. Such a mode could be of magnetic origin, due to, e.g., two-magnon Raman scattering. In low-dimensional systems magnetic modes are observed well above T_N , due to short-range antiferromagnetic order (see, e.g., Ref. 13). However, the highest frequency in the magnon spectrum of $\text{RbFe}(\text{MoO}_4)_2$ as calculated from the value of the exchange field 67 kOe (Ref. 5) and according to the calculations of the spin-wave spectrum¹⁴ is only 6.3 cm^{-1} , by far too low to account for the 80 cm^{-1} Raman mode. As an alternative interpretation, one could suggest the amplitude mode of an incommensurate structural phase transition. The asymmetric reflections observed in the temperature interval below T_c could be due to the appearance of satellites in an incommensurate phase. In that case, the phase transition at $T_c \approx 190$ K into an incommensurate crystal structure would be a precursor of the incommensurate magnetic phase below $T_N = 3.8$ K. However, in all the investigated incommensurate crystals the frequency of the amplitude mode does not exceed 40 cm^{-1} (see, e.g., Ref. 15), which makes the aforementioned interpretation unlikely.

Double molybdates and tungstates with general formula $A^+R^{3+}(\text{MO}_4)_2$ (here A is alkaline atom, Ag, or Tl, R is rare earth, Bi, In, Sc, Ga, Al, Fe, or Cr, M stands for Mo or W) demonstrate a vast variety of crystal structures, exhibit polymorphic transformations and structural phase transitions.^{1,3,7}

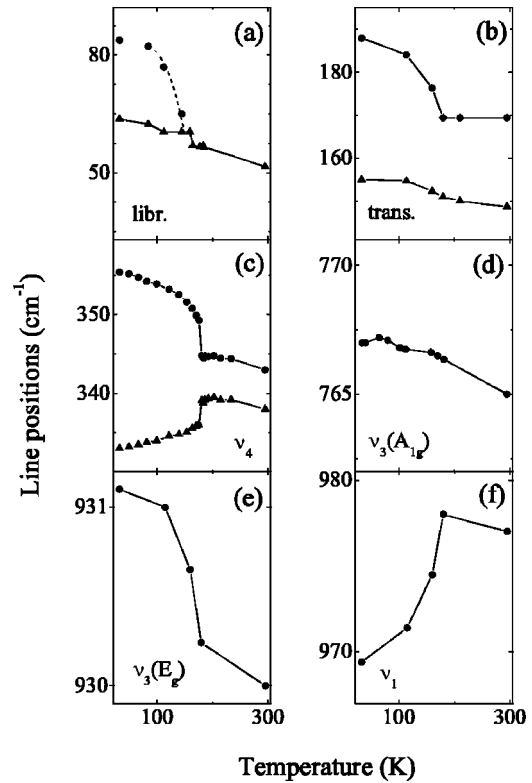


FIG. 8. Temperature dependences of Raman frequencies in $\text{RbFe}(\text{MoO}_4)_2$. Notations refer to the corresponding external motions and internal vibrations of the $(\text{MoO}_4)^{2-}$ entity.

A thorough crystallographic and x-ray structural study on single crystals of $\text{KAl}(\text{MoO}_4)_2$, $\text{KSc}(\text{MoO}_4)_2$, and $\text{KFe}(\text{MoO}_4)_2$ at room temperature revealed a subtle difference between the structures of the first two and the third compound, in spite of a complete identity of their x-ray powder-diffraction patterns.³ The structures of $\text{KR}(\text{MoO}_4)_2$ with $R = \text{Al}$ or Sc belong to the $P\bar{3}m1$ space group whereas the structure of $\text{KFe}(\text{MoO}_4)_2$ is described by the $P\bar{3}c1$ space group. The latter structure is characterized by a pseudoperiod that doubles the c parameter. Successive R layers are not translationally equivalent, as in the case of the $\text{KAl}(\text{MoO}_4)_2$ structure, but are interconnected by a glide plane c . This structural difference is mediated by tiny displacements of the oxygen atoms O2 whereas the positions of other atoms do not change.³ The transformation from $P\bar{3}m1$ to $P\bar{3}c1$ may be considered as a rotation of the two $(\text{MoO}_4)^{2-}$ tetrahedra in the primitive cell of the $P\bar{3}m1$ structure in opposite directions about the C_3 axis. As the O2 oxygen atoms belong also to the FeO_6 octahedra, these rotations lead to the appearance of two differently oriented octahedra in the new $P\bar{3}c1$ primitive cell.

It is possible that the structural phase transition in $\text{RbFe}(\text{MoO}_4)_2$ at $T_c \approx 190$ K is just a transformation from a more symmetric $P\bar{3}m1$ room-temperature structure into a less symmetric $P\bar{3}c1$ low-temperature one, that comprises two differently oriented FeO_6 octahedra.

Table III gives atomic positions and the appropriate irre-

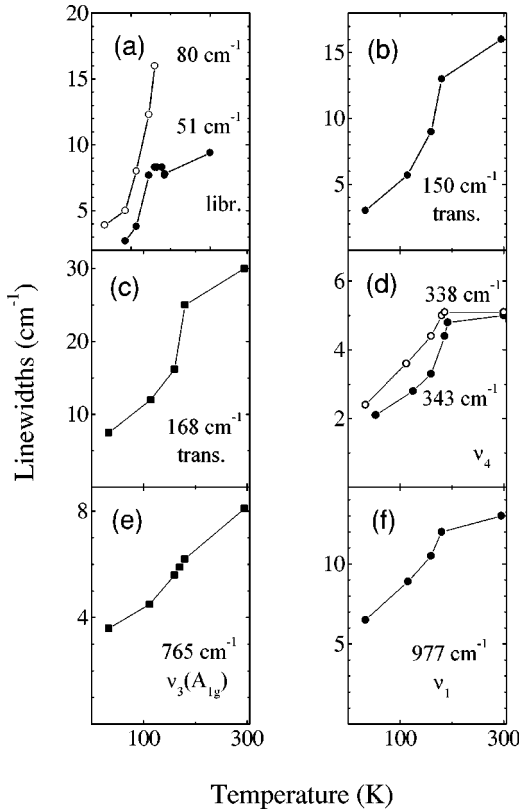


FIG. 9. Linewidths in the Raman spectra of $\text{RbFe}(\text{MoO}_4)_2$ vs temperature.

ducible representations for vibrational modes of the $\overline{P3c1}$ structure. In total, the optical vibrations are

$$\Gamma^{\text{opt}}(\overline{P3c1}) = 5A_{1g}(xx,yy,zz) + 11E_g(xz,yz,xy) + 6A_{2g} + 6A_{1u} + 6A_{2u}(E||z) + 12E_u(E||x,E||y). \quad (2)$$

There are 16 Raman ($5A_{1g} + 11E_g$) and 18 infrared ($6A_{2u} + 12E_u$) modes. Analyzing the vibrational modes in more detail we find that four additional E_g modes and a new doublet $E_g + A_{1g}$ should appear in the region of ν_2 , ν_3 , ν_4 vibrational, translational and, respectively, librational motions of the MoO_4 tetrahedron, due to the additional Davy-

TABLE III. Crystallographic positions and corresponding contributions to the vibrational modes of $\text{RbFe}(\text{MoO}_4)_2$ in the case of $\overline{P3c1}$ structure.

Atom position	Local symm.	Vibrational modes	
Rb	2a	D_3	$A_{2g} + A_{2u} + E_g + E_u$
Fe	2b	C_{3i}	$A_{1u} + A_{2u} + 2E_u$
Mo	4d	C_3	$A_{1g} + A_{1u} + A_{2g} + A_{2u} + 2E_g + 2E_u$
O1	4d	C_3	$A_{1g} + A_{1u} + A_{2g} + A_{2u} + 2E_g + 2E_u$
O2	12g	C_1	$3A_{1g} + 3A_{1u} + 3A_{2g} + 3A_{2u} + 6E_g + 6E_u$

dov splitting in the doubled unit cell. The sixth new E_g mode comes from an activation of Rb motions in the Raman spectra.

The additional Davydov splitting can be small because of a weak interaction between MoO_4 tetrahedra in different layers, so that it is not resolved in Raman spectra. The exception is the additional A_{1g} mode, a Davydov counterpart to the silent A_{2g} librational mode of the $\overline{P3m1}$ structure. We suggest that the extra Raman mode observed below T_c in $\text{RbFe}(\text{MoO}_4)_2$ is just this new A_{1g} librational mode. We have to admit, however, that a new E_g mode associated with motions of Rb is too weak to be observed.

The ESR data enable us to estimate the change of the crystal field below the phase-transition point $T_c = 190$ K, by means of the following considerations. The temperature dependence of the ESR intensity above 10 K corresponds well to the Curie-Weiss law $(T + \Theta_{\text{CW}})^{-1}$ of the static susceptibility with the Curie-Weiss constant $\Theta_{\text{CW}} \approx 25$ K. This value gives an estimation of the exchange interaction energy. Thus, in the temperature range above 100 K, far from critical broadening due to the onset of magnetic order, we consider the ESR linewidth in the high-temperature approximation ($T \gg \Theta_{\text{CW}}$). To show that the crystal field is responsible for the line broadening in $\text{RbFe}(\text{MoO}_4)_2$, we first determine its strength from the evaluation of the resonance field measured at 34 GHz.

The temperature dependence of the resonance field at 34 GHz exhibits a signature typical for the influence of an internal anisotropy field, where the resonance shift is related to the Curie-Weiss law of the susceptibility. The symmetry of the crystal field at the iron site allows only for a uniaxial spin anisotropy with the anisotropy axis parallel to the crystallographic c axis. We choose this axis as the z axis of the local coordinate system. The crystal field partially lifts the degeneracy of the Zeeman levels of the spin- $S = 5/2$ ion Fe^{3+} , already without magnetic field, and leads to a splitting of the ESR spectrum. This effect is usually described in terms of a spin Hamiltonian with a single-ion anisotropy term DS_z^2 , where D is the anisotropy constant.¹⁶ However, the splitting is not observed in $\text{RbFe}(\text{MoO}_4)$, because the influence of the crystal field is effectively averaged by the isotropic Heisenberg exchange interaction. The ESR spectrum is exchange narrowed into a single resonance line, with line shift and broadening resulting from the underlying unnarrowed spectrum.

From the equation of motion we derive the following expressions describing the influence of the crystal field on the temperature dependence of the resonance field H_{res} , analogously to Ref. 17:

$$H_{\text{res}}(c||H) = \frac{h\nu}{g_{||}\mu_B} \left(1 - \frac{2S(S+1)D}{3k_B(T - \Theta_{\text{CW}})} \right)^{-1}, \quad (3)$$

$$H_{\text{res}}(c\perp H) = \frac{h\nu}{g_{\perp}\mu_B} \left(1 + \frac{2S(S+1)D}{3k_B(T - \Theta_{\text{CW}})} \right)^{-1/2}. \quad (4)$$

Here ν is the microwave frequency, h is the Planck constant, μ_B is the Bohr magneton, and k_B is the Boltzmann

constant. Using these two equations, the temperature dependence of the resonance field was well fitted by the g values $g_{\parallel}=1.992(1)$, $g_{\perp}=2.003(1)$, a Curie-Weiss temperature $\Theta_{\text{CW}}=-21(1)$ K, and anisotropy parameter $D/k_B=0.25(1)$ K. The corresponding fit curves are shown as solid lines in the lower frame of Fig. 4. The g value is nearly isotropic, as expected for S -state ions. The Curie-Weiss temperature is in good agreement with that found from the magnetic susceptibility measurements.

Having determined the anisotropy constant D , we can roughly estimate the expected crystal-field contribution to the linewidth, in the framework of the theory of exchange narrowing,^{18,19} by

$$\Delta H_{\text{CF}} \approx \frac{1}{g\mu_B} \frac{D^2}{J}. \quad (5)$$

With the Heisenberg exchange coupling JS_iS_j of a spin S_i to its six nearest neighbors S_j in the basal plane, we obtain the corresponding exchange integral from the Curie-Weiss temperature as $J/k_B \approx \Theta_{\text{CW}}/(6S^2) \approx 0.67$ K. Inserting the values for D and J in Eq. (5) yields $\Delta H_{\text{CF}} \approx 700$ Oe, which is the right order of magnitude.

Note that the values of D and J determined above agree very well with those obtained independently from the magnetization and ESR measurements in the antiferromagnetically ordered phase⁵, where the anisotropy field $H_A = DS/(g\mu_B) = 5$ kOe and the exchange field $H_E = 6JS/(g\mu_B) = 67$ kOe give $D/k_B = 0.27$ K and $J/k_B = 0.6$ K, respectively.

Concerning other possible contributions to the linewidth, symmetric anisotropic exchange and Dzyaloshinsky-Moriya interaction can be neglected. Indeed, the orders of magnitudes of the characteristic energies of these interactions are $(\Delta g/g)^2 J$ and $(\Delta g/g)J$, respectively, where $(\Delta g/g)$ is the relative anisotropy of the g factor.²⁰ Due to the nearly isotropic g factor observed in our measurements the magnitudes of the interactions mentioned above are negligible in comparison with D . Hyperfine interaction can be neglected as well, because the nuclear spins of ⁵⁶Fe and surrounding ¹⁶O are zero and the other nuclei are too far away. Only the dipole-dipole interaction gives an additional contribution in the presence of the exchange interaction, and can be written in the form

$$\Delta H_{DD} \approx \frac{3g^3\mu_B^3 S(S+1)}{Jr^6}. \quad (6)$$

With the nearest-neighbor distance $r=a=5.69$ Å, this yields $\Delta H_{DD} \approx 50$ Oe, which is still small compared to the experimentally observed linewidth. Hence the linewidth is

indeed dominated by the single-ion anisotropy. This is also in agreement with the observed angular dependence of the linewidth. Namely, for the magnetic field applied parallel to the direction of the anisotropy axis the ESR line is twice as large as for the magnetic field applied perpendicular to this direction.

Transformation of the crystal structure causes in a natural way a change of the crystal field in the surrounding of Fe^{3+} ions. Using the above consideration of the ESR linewidth we deduce from the 4% change of the linewidth in the temperature range between 180 and 190 K that the crystal field is increased by about 2% below the transition point. The increase of the crystal field strength may be caused by the distortion of the FeO_6 octahedra combined with the rotations of MoO_4 , because they are sharing vertices.

V. CONCLUSIONS

We have carried out x-ray powder diffraction, ESR, and Raman scattering measurements on $\text{RbFe}(\text{MoO}_4)_2$ at different temperatures. The temperature dependence of the unit-cell parameters a and c display a peculiarity between 200 and 180 K. The temperature dependences of the resonance fields demonstrate small but distinct steps at $T_c=190$ K. In the Raman spectra, all nine modes predicted by the group-theoretical analysis were observed for the temperatures higher than T_c . Below T_c , these modes shift and narrow markedly and a new low-frequency mode appears. Raman, ESR, and x-ray powder-diffraction data point to a second order structural phase transition at $T_c \approx 190$ K. Based on the changes in the Raman and ESR spectra below T_c , we suggest that the 190 K phase transition is mediated by rotations of the MoO_4 tetrahedra, resulting in a symmetry lowering from $P3m1$ to $P3c1$. From the experimental temperature dependencies of the ESR field above 10 K we derived the g -factor values $g_{\parallel}=1.992$ and $g_{\perp}=2.003$, the Curie-Weiss constant $\Theta_{\text{CW}}=-21$ K, and the single-ion anisotropy constant $D/k_B=0.25$ K.

ACKNOWLEDGMENT

The authors kindly acknowledge D. Vieweg for making x-ray and SQUID measurements, and V.N. Glazkov and S.S. Sosin for discussions. This work was supported by INTAS, Grant No. 99-0155 and by the Russian Foundation for Basic Research, Grants No. 01-02-16329 and 01-02-17557, by Deutsche Forschungsgemeinschaft (DFG) via Grant No. SFB 484 and the joint Grant Nos. DFG-RFBR, 436 RUS 113/628, by German BMBF under Contract No. VDI/EKM 13N6917, and by the Netherlands Foundation for Fundamental Research on Matter (FOM).

¹P.V. Klevtsov and R.F. Klevtsova, Zh. Strukt. Khim. **18**, 419 (1977).

²V.K. Trunov and V.A. Efremov, Zh. Neorg. Khim. **16**, 1082 (1971).

³R.F. Klevtsova and P.V. Klevtsov, Kristallografiya **15**, 953 (1970).

⁴T. Inami, Y. Ajiro, and T. Goto, J. Phys. Soc. Jpn. **65**, 2374 (1996).

⁵L.E. Svistov, A.I. Smirnov, L.A. Prozorova, O.A. Petrenko, L.N.

- Demianets, and A.Ya. Shapiro, Phys. Rev. B **65**, 094434 (2003).
- ⁶G. Gasparovich, M. Kenzelmann, C. Broholm, L. N. Demianets, and A. Ya. Shapiro, APS March meeting 2003, Abstract N31.004.
- ⁷A.I. Otko, L.N. Pelikh, L.V. Povstyanyi, N.M. Nesterenko, P.S. Kalinin, and A.I. Zvyagin, Izv. Akad. Nauk SSSR, Ser. Fiz. **39**, 697 (1975).
- ⁸I.E. Dzyaloshinsky, Zh. Éksp. Teor. Fiz. **46**, 1420 (1964) [Sov. Phys. JETP **19**, 960 (1964)].
- ⁹Z. Seidov, H.-A. Krug von Nidda, J. Hemberger, A. Loidl, G. Sultanov, E. Kerimova, and A. Panfilov, Phys. Rev. B **65**, 014433 (2001).
- ¹⁰D.L. Rousseau, R.P. Bauman, and S.P.S. Porto, J. Raman Spectrosc. **10**, 253 (1981).
- ¹¹K. I. Petrov, M. E. Poloznikova, H. T. Sharipov, and V. V. Fomichev, *Vibrational Spectra of Molybdates and Tungstates* (Fan, Tashkent, 1990) (in Russian).
- ¹²R.H. Busey and O.L. Keller, Jr., J. Chem. Phys. **41**, 215 (1964).
- ¹³M. G. Cottam and D. J. Lockwood, *Light Scattering in Magnetic Solids* (Wiley & Sons, New York, 1986).
- ¹⁴E. Rastelli and A. Tassi, J. Phys.: Condens. Matter **8**, 1811 (1996).
- ¹⁵M. V. Klein, in *Light Scattering Near Phase Transitions*, edited by H. Z. Cummins and A. P. Levanyuk (North-Holland, Amsterdam, 1983), p. 503.
- ¹⁶S. A. Altshuler and B. M. Kosyrev, *Electron Paramagnetic Resonance in Compounds of Transition Elements* (Nauka, Moscow, 1972).
- ¹⁷J. Deisenhofer, M.V. Eremin, D.V. Zakharov, V.A. Ivanshin, R.M. Eremina, H.-A. Krug von Nidda, A.A. Mukhin, A.M. Balbashov, and A. Loidl, Phys. Rev. B **65**, 104440 (2002).
- ¹⁸P.W. Anderson and P.R. Weiss, Rev. Mod. Phys. **25**, 269 (1953).
- ¹⁹R. Kubo and K.J. Tomita, J. Phys. Soc. Jpn. **9**, 888 (1954).
- ²⁰T. Moriya, Phys. Rev. **120**, 91 (1960).